



Published in final edited form as:

Acta Neuropathol. 2018 May ; 135(5): 711–726. doi:10.1007/s00401-018-1824-0.

Mechanical disruption of the blood–brain barrier following experimental concussion

Victoria E. Johnson¹, Maura T. Weber¹, Rui Xiao², D. Kacy Cullen^{1,3,6}, David F. Meaney³, William Stewart^{4,5}, and Douglas H. Smith¹

¹Department of Neurosurgery, Penn Center for Brain Injury and Repair, Perelman School of Medicine, University of Pennsylvania, 105 Hayden Hall, 3320 Smith Walk, Philadelphia, PA 19104, USA

²The Department of Biostatistics, Epidemiology and Informatics, University of Pennsylvania, Philadelphia, PA 19104, USA

³Department of Bioengineering, University of Pennsylvania, Philadelphia, PA 19104, USA

⁴Department of Neuropathology, Queen Elizabeth University Hospital, Glasgow G51 4TF, UK

⁵Institute of Neuroscience and Psychology, University of Glasgow, Glasgow G12 8QQ, UK

⁶Corporal Michael J. Crescenz VAMedical Center, Philadelphia, PA 19104, USA

Abstract

Although concussion is now recognized as a major health issue, its non-lethal nature has limited characterization of the underlying pathophysiology. In particular, potential neuropathological changes have typically been inferred from non-invasive techniques or post-mortem examinations of severe traumatic brain injury (TBI). Here, we used a swine model of head rotational acceleration based on human concussion to examine blood–brain barrier (BBB) integrity after injury in association with diffuse axonal injury and glial responses. We then determined the potential clinical relevance of the swine concussion findings through comparisons with pathological changes in human severe TBI, where post-mortem examinations are possible. At 6–72 h post-injury in swine, we observed multifocal disruption of the BBB, demonstrated by extravasation of serum proteins, fibrinogen and immunoglobulin-G, in the absence of hemorrhage or other focal pathology. BBB disruption was observed in a stereotyped distribution consistent with biomechanical insult. Specifically, extravasated serum proteins were frequently observed at interfaces between regions of tissue with differing material properties, including the gray–white boundary, periventricular and subpial regions. In addition, there was substantial overlap of BBB disruption with regions of axonal pathology in the white matter. Acute perivascular cellular uptake of blood-borne proteins was observed to be prominent in astrocytes (GFAP-positive) and neurons

Douglas H. Smith smithdou@pennmedicine.upenn.edu.

The content is solely the responsibility of the authors and does not necessarily represent the official views of the Department of Defense, National Institutes of Health, or Department of Veterans Affairs.

Electronic supplementary material The online version of this article (<https://doi.org/10.1007/s00401-018-1824-0>) contains supplementary material, which is available to authorized users.

Conflict of interest The authors declare that they have no conflict of interest.

(MAP-2-positive), but not microglia (IBA1-positive). Parallel examination of human severe TBI revealed similar patterns of serum extravasation and glial uptake of serum proteins, but to a much greater extent than in the swine model, attributed to the higher injury severity. These data suggest that BBB disruption represents a new and important pathological feature of concussion.

Keywords

Mild traumatic brain injury; Concussion; Blood–brain barrier; Fibrinogen; Gliosis; Biomechanics

Introduction

Concussion is now recognized as a major health issue, with many millions of cases reported worldwide each year [11, 18, 61]. Indeed, although alternatively referred to as mild traumatic brain injury (mTBI), for many there is nothing ‘mild’ about concussion, with approximately 15% of patients suffering persisting neurocognitive dysfunction [68, 70]. Moreover, an increasing number of reports link exposure to repetitive concussions with progressive neurodegeneration, including ‘chronic traumatic encephalopathy’ (CTE) [33, 57, 83].

Despite growing public alarm regarding the aftermath of concussion, there remains no consensus on the underlying pathophysiology of the injury. In part, this is due to the limited availability of human post-mortem brain tissue for examination from this typically non-lethal injury. As such, concussion remains in part defined by an absence of the overt brain pathologies characteristic of higher levels of TBI, including, hematoma, contusion or marked brain swelling [51]. However, emerging experimental and clinical data indicates that concussion may share one of the most consistently observed pathologies of moderate and severe TBI, diffuse axonal injury (DAI).

Across all injury severities, DAI is thought to stem from the viscoelastic nature of the brain under *dynamic* mechanical loading during head rotational acceleration [3, 26, 36, 37, 43, 58, 84, 86, 87]. Potentially due to their highly structured organization in tracts and unique anatomic architecture, axons appear especially vulnerable to rapid brain tissue deformation during TBI. This has been demonstrated in a swine model of concussion that employs head rotational acceleration parameters scaled to human concussion [17, 44]. Neuropathological analysis of the injured swine brains identified selective, multifocal regions of axonal pathology throughout the white matter very similar in appearance to characteristic DAI observed at autopsy after severe TBI in humans [44]. In addition, a growing number of reports using advanced neuroimaging and fluid biomarker analyses lend further support for DAI as a key pathological substrate of concussion in both humans and animal models [12, 55, 59, 76, 81, 94, 95].

Intriguingly, emerging evidence suggests that other brain structures also suffer mechanical injury during concussion, which like DAI typically are invisible to conventional, noninvasive examination. In particular, while by definition there is no focal hemorrhage in concussion, techniques such as dynamic contrast enhanced (DCE) MRI have demonstrated contrast accumulation in the brains of football players [93], suggesting there is subtle disruption of

the cerebral vasculature affecting the integrity of the blood–brain barrier (BBB). In addition, in previous preclinical studies, BBB dysfunction has been observed in the absence of other significant neuropathologies following an open-skull, direct impact model of TBI in cats [66, 67]. In these studies, BBB permeability was demonstrated to occur via multiple routes including increased transcytosis as well as hypertension-induced endothelial breakdown. Furthermore, autopsy studies in humans have demonstrated acute and long-lasting disruption of BBB integrity as a common neuropathological finding after just a single moderate or severe TBI [34]. However, the specific contribution of isolated mechanical forces on the BBB, including rotational forces common to concussion, has yet to be explored directly.

Here, we evaluated potential BBB disruption following injury in the swine head rotational acceleration model of concussion. We found acute and marked BBB leakage at levels of injury insufficient to cause hemorrhage. Detailed neuropathological examination revealed that BBB permeability occurred in a pattern and distribution consistent with a biomechanically induced pathology and was associated with an acute astroglial response. Parallel studies of human cases of moderate and severe TBI confirmed neuropathological features similar to those found in the swine concussion model, though with evidence of more extensive BBB disruption, consistent with previous observations. Together, these data indicate that, in addition to DAI, BBB dysfunction may also be an important pathology of concussion.

Materials and methods

Experimental design

We hypothesized that dynamic forces caused by rapid head rotational acceleration–deceleration in adult swine will induce acute extravasation of blood-borne proteins into the brain parenchyma that are detectable via immunohistochemistry (IHC). In a controlled laboratory experiment, 6-month-old (adult) Hanford miniature swine underwent the rotational acceleration model of TBI under general anesthesia and survived for 6 h ($n = 3$), 48 h ($n = 2$) and 72 h ($n = 4$), and were compared with shams ($n = 3$). Based on previous data [44] the proposed number of animals was expected to provide significant power, specifically where the neuropathological outcome was anticipated to be absent in sham animals. All histological experiments, analyses and quantification were performed blind to the injury status of the animal.

Rotational acceleration model of concussion

All animal experiments were conducted in accordance with protocols approved by The University of Pennsylvania Institutional Animal Care and Use Committee and in accordance with the NIH Guide for the Care and Use of Laboratory Animals.

Six-month-old female Hanford miniature swine were subjected to an established concussion model that induces injury via forces caused by rotational acceleration/deceleration due to pure impulsive centroidal head rotation [17, 44, 58, 71, 82, 85]. For TBI in humans, the size of the brain is critical as significant mass effects between regions of tissue can create high strains during dynamic brain deformation during rapid accelerations [36, 37, 54].

Accordingly, injury parameters were scaled up relative to brain mass to create the mechanical loading of brain tissue relevant to that which occurs in human TBI [36, 37, 54, 58, 89]. Notably, in this model, there is an absence of any head impact or forces arising from linear acceleration/deceleration.

Following the induction of anesthesia using 0.4 mg/kg midazolam IM and 5% inhaled isoflurane, animals were intubated and anesthesia maintained via 2.5% inhaled isoflurane. The HYGE pneumatic actuator device was used to induce rapid head rotation. Specifically, the HYGE actuator generates linear motion via the triggered release of pressurized nitrogen. This linear motion is then converted to angular motion via custom-designed linkage assemblies to induce rotation over 20 ms. Rotational kinematics were recorded using angular velocity transducers (Applied Technology Associates) mounted to the linkage sidearm coupled to a National Instruments data acquisition system running custom LabView software (10 kHz sampling rate). In this fashion, we produced pure impulsive centroidal head rotation of up to 110° in the coronal plane with peak angular velocity of 225–250 rad/s. Animals were recovered from anesthesia and returned to the housing facility. While the procedure is non-surgical, preemptive analgesia was provided post-injury in the form of 0.1–3 mg of Buprenex (slow release preparation) SQ and acetaminophen 50 mg/kg PR. Sham animals were also euthanized 72 h after being subjected to identical procedures absent head rotation.

At the study endpoint, all animals were deeply anesthetized and transcardially perfused using chilled heparinized saline (2 L) followed by 10% neutral buffered formalin (NBF) (8 L). Perfusions were performed at standardized pressures calibrated for the provision of adequate fixation and the absence of any structural damage to the vasculature that would permit artefactual extravasation of serum proteins. This was verified histologically (described below) and fixation was sufficient to permit quality tissue morphology and immunoreactivity. Brains were subsequently postfixed for 7 days in 10% NBF, sectioned into 5 mm blocks in the coronal plane and processed to paraffin using standard techniques.

Human post-mortem acute severe TBI cohort: demographic and clinical data

Since uncomplicated concussion is typically non-lethal, scarce cases come to autopsy examination. Therefore, postmortem brain tissue from patients who died following single severe TBI was examined to determine if there were shared features in the distribution of serum protein extravasation and the cellular response to **BBB** breakdown between human autopsy material and our swine injury model across injury severities. All tissue was obtained from the Glasgow TBI Archive, Department of Neuropathology, Queen Elizabeth University Hospital, Glasgow, UK. Tissue was acquired at routine diagnostic autopsy and approval for use was granted by the NHS Greater Glasgow and Clyde Bio-repository Governance Committee.

TBI cases were selected to include patients with survival times ranging from 6 to 72 h following acute severe TBI ($n = 12$). Detailed reports from the diagnostic autopsy and/or forensic reports were available for all cases and indicated a history of a single severe TBI, supported by autopsy findings. TBI cases were compared to material from age/sex-matched controls ($n = 7$) acquired at routine diagnostic post-mortem at the same institution. Controls

had no documented history of TBI. Full clinical and demographic information, including age, sex and cause of death, is provided for all groups in Table 1.

Human brain tissue preparation

For all examinations, the intact brain was immersed in 10% formol saline at autopsy and fixed for at least 3-weeks prior to dissection. Sampling using a standardized protocol and paraffin embedding was performed as described previously [31]. Analyses were performed using hemi-coronal sections of the parasagittal cortex at the level of the mid-thalamus to include the cingulate gyrus, corpus callosum and superior frontal gyrus. This region was selected given its midline location and known susceptibility to injury [1, 2, 42, 43, 49].

Single immunohistochemical labeling

Human and swine tissue was examined for extravasation of the serum protein fibrinogen (FBG) and axonal pathology using IHC. Following deparaffinization and rehydration, human and swine tissue sections were immersed in aqueous hydrogen peroxide (15 min) to quench endogenous peroxidase activity. Antigen retrieval was performed in a microwave pressure-cooker with immersion in preheated Tris EDTA buffer. Subsequent blocking was achieved using 1% normal horse serum (Vector Labs, Burlingame, CA) in Optimax buffer (BioGenex, San Ramon, CA) for 30 min. Incubation with the primary antibodies was performed overnight at 4°C. Specifically, to identify axonal pathology in human and swine tissue, sections were labeled with an antibody reactive for the N-terminal amino acids 66–81 of the amyloid precursor protein (APP) (Millipore, Billerica, MA) at 1:80 k permitting visualization of APP accumulating within transport-interrupted axonal bulbs or swollen and tortuous varicosities along the length of damaged axons. In addition, adjacent sections were incubated with antibodies specific for the serum protein FBG including rabbit polyclonal antibodies targeting the full-length swine FBG at 1:5 k (Abcam, Cambridge, MA) and human FBG at 1:17.5 K (Dako, Carpinteria, CA). FBG does not normally accumulate in the brain parenchyma under physiologic conditions. After rinsing, sections were incubated with the appropriate biotinylated secondary antibody for 30 min (Vector Labs, Burlingame, CA), followed by avidin–biotin complex (Vectastain Universal Elite kit, Vector Labs, Burlingame, CA). Finally, visualization was achieved using 3,3'-diaminobenzidine (DAB) (Vector Labs, Burlingame, CA) and counter-staining with haematoxylin performed.

Positive control tissue for APP IHC included sections of swine tissue with previously established DAI. Positive control tissue for FBG IHC included a section of swine brain tissue with contusional injury, and thus overt BBB disruption. Omission of primary antibodies was performed on the same material to control for non-specific binding.

Multiple antigen labeling

Immunoenzymatic double labeling—Sections were examined to directly compare the pattern and distribution of FBG extravasation with that of axonal pathology in swine. Specifically, APP staining was first performed using DAB visualization as above. The same sections were subsequently incubated with rabbit anti-FBG antibody (1:3.5 K) for 20 h at 4°C. Detection was achieved via the ImmPRESS™-AP anti-rabbit IgG (alkaline phosphatase) polymer detection kit (Vector Labs, Burlingame, CA) followed by the Vector

blue alkaline phosphatase substrate kit (Vector Labs, Burlingame, CA). After rinsing, slides were coverslipped using aqueous mounting medium (Dako, Carpinteria, CA).

Immunofluorescent (IF) labeling—Double and triple IF labeling was performed in swine tissue to (1) compare the extravasation of FBG with that of another blood-borne protein IgG in a section of tissue at the level of the basal ganglia at the level of the head of caudate nucleus in all cases and; (2) determine the cell types associated with the uptake of FBG/IgG in all sections where observed on single labeling IHC.

Following deparaffinization and rehydration, antigen retrieval and blocking was performed as above. Primary antibodies were applied serially for 20 h (4°C) and were specific for FBG (Abcam, Cambridge, MA, 1:3 K), glial fibrillary acidic protein (GFAP) (Millipore, Billerica, MA; 1:8 K), ionized calcium-binding adaptor molecule 1 (IBA-1), and microtubule-associated protein 2 (MAP2) (Abcam, Cambridge, MA; 1:2 K). After rinsing, the corresponding Alexa Fluor (Invitrogen, Carlsbad, CA) secondary antibody was applied at 1:500 in a 2% species-specific blocking solution for 2 h at room temperature. For the identification of IgG, a goat anti-swine IgG conjugated with Alexa 488 (Jackson ImmunoResearch, PA; 1:20) was applied. Serial sections of positive control tissue (contused tissue) were subjected to the entire procedure with the omission of subsets of primary antibodies to control for non-specific immunofluorescence. Negative controls included individual omission of primary antibodies to control for non-specific binding. Following rinsing, all double fluorescent-immunolabeled sections were coverslipped using an aqueous mounting medium (Dako, Carpinteria, CA) and visualized using a Nikon A1RSi Laser Scanning Confocal (Nikon, Tokyo, Japan). High resolution confocal scanning was performed at 0.5 μm increments through the full depth of the tissue sections and image reconstruction achieved using Nikon Elements AR.

Analysis and quantification of immunohistochemical findings

All neuropathological assessment and quantification was performed blinded to the injury status of animals by 2 independent examiners and inter-rater reliability was determined. Routine H&E staining was performed on serial sections for all brain regions examined (see below).

Extent and distribution of FBG extravasation—All tissue examinations were performed on 8 μm wholebrain coronal paraffin sections at 5 brain levels including: (1) the frontal cortex at 5 mm from the frontal pole, including prefrontal cortex; (2) the basal ganglia at the level of the head of caudate nucleus; (3) the anterior hippocampus; (4) the posterior hippocampus at the level of the posterior commissure; and (5) the medulla. Levels were selected to incorporate a wide sampling spanning the rostrocaudal extent of the entire brain.

For each animal, FBG labelled whole-brain sections from each of these 5 levels (see Fig. 2a for examples of brain levels examined) were subjected to high resolution scanning at 20 \times magnification using the Aperio ScanScope and viewed using associated Aperio ImageScope software (Leica Biosystems, Wetzlar, Germany). These digital images were reviewed by 2 independent observers (VJ and MW) each of whom manually outlined all regions of

extravasated FBG to generate detailed maps of BBB disruption (Fig. 2). This was achieved using the annotation tool on the Aperio ImageScope software. These subsequent outlines then permitted the quantification of the percentage area of FBG immunoreactivity for each hemisphere (across all 5 brain levels) per animal.

Quantifying regional overlap between FBG extravasation and axonal pathology in swine—The pattern and distribution of axonal pathology as identified by APP immunohistochemistry has previously been characterized in the non-impact rotational acceleration injury swine model of mild TBI used in this study [44].

To determine the potential relationship between axonal pathology and BBB disruption, tissue dual-labelled for APP (axonal pathology) and FBG were examined. Animals with the survival of 48–72 h post-TBI were selected to encompass the maximal extent of axonal pathology, which is identifiable due to the abnormal accumulation of APP secondary to a failure of axonal transport.

Dual-labelled coronal sections for all cases at the level of the basal ganglia at the level of the head of caudate nucleus (Fig. 3a, b) were selected and, as above, underwent high resolution digital scanning at 20× magnification using the Aperio ScanScope and viewed using associated Aperio ImageScope software (Leica Biosystems, Wetzlar, Germany).

The entire region of white matter above the level of the corpus callosum for each animal/section in both hemispheres was selected for examination and has previously been shown to be a region where axonal pathology is stereotypically observed [44]. Within this region, injured axons were identified and defined as those that were APP positive axonal profiles with an injured morphology including (1) terminal axonal swellings or axonal bulbs, formerly known as retraction balls, and (2) axons with a beaded or fusiform morphology representing multiple points of apparent transport interruption as has been historically described [27, 28, 42, 43, 77, 88]. Upon identification, injured axons were tagged using the annotation tool in the Aperio ImageScope software. To determine the percentage of axons regionally associated with BBB disruptions, all axons were reviewed and designated as either (1) existing in a region of white matter with associated FBG extravasation or (2) existing in a regions where FBG immunoreactivity was absent.

Human tissue neuropathological analyses—For human tissue studies, the extent of FBG extravasation was classified using standard semi-quantitative assessments and designated in a blinded fashion as: 0 = absent, 1 = minimal, 2 = moderate, or 3 = extensive pathology based on the frequency and intensity of immunoreactivity as previously described [34]. Score 3 (extensive) represents sections with > 50% of the section being FBG immunoreactive. Representative examples are shown in Supplementary Fig. 2. This scoring was representative of the entire hemi-coronal section of the parasagittal cortex at the level of the mid-thalamus to include the cingulate gyrus and corpus callosum. The presence or absence of axonal pathology was noted.

Statistical analyses

Statistical analyses for IHC quantification were performed using GraphPad Prism statistical software (GraphPad Software Inc. La Jolla, CA). Differences in the mean of the percentage area of FBG immunoreactivity were assessed using the two-sample *t* test for all comparisons. Differences were considered significant if $p < 0.05$.

The Intraclass Correlation Coefficient (ICC) was used to determine inter-rater reliability of quantitative measurements of IHC findings using IBM SPSS Statistics (IBM Corporation, Armonk, NY).

Results

Isolated head rotational acceleration results in a clinical presentation consistent with concussion

Following the rotational acceleration model of concussion and subsequent withdrawal of isoflurane, all animals mobilized rapidly, were fully conscious and alert, mental status was unaltered and normal feeding and drinking behavior resumed within 1–2 h. Consistent with the clinical presentation of mild TBI, no animals displayed evidence of focal neurological deficit. In all animals, neurological examination was normal and animals displayed normal posture, tone, gait, power, sensation, proprioception and cranial nerve examination where possible to examine.

Neuropathological characterization of trauma-associated pathologies was performed following survival of 6 h ($n = 3$), 48 h ($n = 2$) and 72 h ($n = 4$) post-injury and compared with shams ($n = 3$). As previously reported [44], brains were normal on gross examination and indistinguishable from shams at all time points post-injury. Consistent with clinical concussion, there was no evidence of any focal pathology, including hemorrhage. The brain hemispheres were symmetrical with no evidence of swelling or raised intracranial pressure (ICP). H&E staining confirmed an absence of any focal hemorrhagic or ischemic foci in any animals.

IHC specific for APP revealed swollen and morphologically altered axons consistent with transport-interruption secondary to axonal cytoskeletal damage and indistinguishable from that observed in human DAI [1–3, 27, 28, 42, 77]. DAI was observed in injured animals in all brain levels examined in a stereotyped multifocal distribution consistent with biomechanical forces as previously described in detail [44] and discussed below.

Experimental concussion results in acute BBB disruption

Multifocal FBG extravasation into the brain parenchyma was observed at 6–72 h following a single, rapid rotation in swine as perivascular FBG immunoreactivity in both white and gray matter in injured animals, but was observed minimally in shams (Fig. 1a–i). Further, detailed mapping of FBG extravasation in multiple whole-brain coronal sections revealed BBB leakage in a stereotyped, multifocal distribution consistent with a biomechanical etiology. Specifically, structural interfaces within the brain were preferentially affected, with the evidence of BBB disruption typically observed at gray–white interfaces, in periventricular

regions (Figs. 1d–f, 2c, e) and at subpial zones within the cortex, often towards the dorsal surface anteriorly (Figs. 1h, 2c). Occasionally, inflection points in the brain architecture were also affected, including cortical sulci and the lateral aspect of the parahippocampal cortex where it meets the inferior temporal gyrus (Fig. 1f), further supporting a biomechanical etiology. In all cases, the hippocampus was affected bilaterally, with prominent FBG extravasation at the interface between the hilus/molecular layer and the dentate gyrus and the vessels of the hippocampal fissure (Fig. 1g). Finally, FBG extravasation was observed in the thalamus at all time points (Fig. 2d).

Quantification of the mean percentage area of FBG immunoreactivity in each hemisphere across 5 coronal sections was minimal in sham animals [left hemisphere: $0.18 \pm 0.01\%$; right hemisphere: $0.29 \pm 0.05\%$]. In comparison with sham, the mean percentage area of FBG immunoreactivity was increased in both hemispheres at 6 h [left hemisphere: $4.39 \pm 2.30\%$ ($p = 0.03$), right hemisphere $3.87 \pm 1.88\%$ ($p = 0.03$)], and at 48 h post-concussion [left hemisphere: $1.16 \pm 0.46\%$ ($p = 0.02$), right hemisphere $1.31 \pm 0.05\%$ ($p = 0.0002$)]. By 72 h post-concussion, FBG immunoreactivity remained increased versus shams in the left hemisphere [$2.30 \pm 1.32\%$ ($p = 0.04$)], with a trend to increased staining in the right hemisphere [$2.50 \pm 2.27\%$ ($p = 0.16$)] (Fig. 1i). No difference in the extent of FBG immunoreactivity was observed between TBI groups at 6, 48 and 72 h survival ($p > 0.05$). Interrater reliability between observers was excellent with an ICC of 0.98.

Notably, while the extent of FBG immunoreactivity did not differ between hemispheres ($p > 0.05$), a stereotyped hemispheric asymmetry was observed at all three time points and was highly consistent among animals. Specifically, in rostral brain regions (Fig. 2a, c), the left hemisphere (leading hemisphere during coronal rotation) displayed an increased density of extravasated FBG closer to the midline, including extensive leakage at the dorsolateral aspect of the lateral ventricle. This was in contrast to the right (non-leading) hemisphere, where more extensive extravasation was observed closer to the brain surface, including the digitate white matter and gray matter of the insular cortex and primary somatosensory cortex (Fig. 2c).

Immunoglobulin (IgG) IHC revealed perivascular extravasation consistent in both extent and distribution with that of FBG in swine (Fig. S1). Additional double immunofluorescent labeling in a subset of sections confirmed co-localization of FBG and IgG, consistent with evidence of BBB disruption leading to global leakage of large, blood-borne proteins, versus being a FBG specific phenomenon (Fig. S1).

Regional overlap of BBB disruption and axonal pathology following experimental concussion

The spatial relationship between axonal pathology and BBB disruption in swine was revealed by examining whole-brain sections at 48–72 h post-concussion at the level of the head of caudate nucleus (Level b; Fig. 3) labeled with both APP and FBG (multiple immunoenzymatic labeling) and compared to sham animals.

Distinct axonal profiles with an injured morphology, including terminal swellings, beading and intact fusiform profiles were present in a stereotypical, multifocal distribution affecting

the subcortical and periventricular white matter and midline structures of all injured animals, consistent with previous reports [44] (Fig. 3b). Notably, mapping of APP positive injured axons revealed overlap between regions of high-density axonal pathology and extensive FBG extravasation in white matter (Fig. 3a, b). However, although frequent, this overlap between APP positive axonal profiles and regions of FBG extravasation in white matter was not absolute (Fig. 3c, e–k). Specifically, though 62.8% (SD 1.8%) and 60.6% (SD 9.3%) of APP positive axons at 48 and 72 h, respectively, fell within a region of co-incident FBG extravasation, the remaining axons did not (Fig. 3c). There was no difference between time points ($p = 0.8$). FBG extravasation was also frequently observed in the absence of any axonal pathology in both white and gray matter (Fig. 3g, k).

Cellular uptake of FBG occurs acutely following experimental concussion

Single labeling IHC revealed that, following concussion in swine, in addition to parenchymal FBG immunoreactivity, staining was also present in cellular structures within regions of high extravasation (Fig. 4). Morphologically, these cells appeared consistent with astrocytes and neurons, confirmed in subsequent double and triple immunohistochemical labeling with GFAP (Fig. 4f–i) and MAP2 (Fig. 4j, k). In contrast, only very occasional microglia (IBA-1 positive) were observed co-labeled with FBG, typically closely adjacent to the vessel (Fig. 4h, i). High resolution confocal microscopy demonstrated this FBG immunoreactivity was within neurons and astrocytes, rather than confined to the cell surface, indicating internalization of the protein. All studies were repeated with IgG, which showed a similar pattern of neuronal and astrocytic uptake (Fig. S1).

APP and FBG IHC following human severe TBI: comparisons with experimental concussion

Following severe human TBI, APP IHC revealed axonal pathology in all TBI cases in a pattern and distribution consistent with DAI, with axonal profiles observed individually scattered or in small clusters, indistinguishable to that observed following concussion in swine [42, 43]. However, in contrast with the concussion model, other cases displayed additional superimposed, widespread waves of axonal APP immunoreactivity in keeping with axonal pathology as a result of the vascular complications of raised intracranial pressure [23, 25, 32, 35, 42, 69]. This compared to human controls where just 1 of 7 cases displayed axonal pathology in a pattern and distribution in keeping with hypoxic/ ischemic injury, likely indicative of an agonal event near the time of death [23, 25, 32, 35, 42, 69].

Moderate or extensive FBG immunostaining was observed in all but one TBI case, consistent with previous reports (Fig. 5) [34, 52]. This compared to controls in which there was less extensive FBG immunoreactivity, with just 1 case showing extensive, 1 moderate and 5 minimal extravasation (Fig. 5a), again in keeping with previous descriptions [34, 52]. Despite the more widespread and extensive FBG immunoreactivity in human severe TBI, consistent with observations in swine studies, there was increased FBG immunoreactivity adjacent to subpial vessels in the superficial layers of the cortex (Fig. 5c, d), as well as at the interface between cortical gray and underlying white matter (Fig. 5e).

Furthermore, both neuronal and glial uptake of FBG was also observed in TBI and control cases (Fig. 5e–g), typically in regions with high parenchymal FBG extravasation. The extent of this cellular uptake was frequently extensive and widespread in human TBI cases, with immunoreactive astrocytes often present at the cortical surface (Fig. 5g).

Discussion

Using a swine model of concussion delivering pure head rotational acceleration and based on the kinematics of human concussion, we found evidence of multifocal BBB disruption shortly after injury. Extravasation of serum proteins was identified in a distribution that coincided with brain regions previously predicted to undergo greatest tissue deformation during injury. While this included overlap with areas of axonal pathology in the white matter, BBB disruption was also found independent of axonal injury throughout the gray matter. Notably, extravasated serum proteins were observed within astrocytes and neurons in proximity to regions of BBB disruption shortly after injury, suggesting rapid uptake by these cells. These data indicate that acute dysfunction of the neurovascular unit may be a common pathological feature of concussion.

While a wide range of pathologies have been characterized in human tissue studies from patients exposed to moderate or severe TBI [30], the rarity of post-mortem examination following concussion has meant that current understanding of the pathophysiology of the injury is based largely on indirect and non-invasive studies in vivo. Moreover, although there are multiple rodent models of ‘mild’ TBI, there is debate regarding their fidelity to replicate the biomechanics and pathophysiology of human concussion. In particular, the relatively large and gyrencephalic human brain endures substantial mass effects during head rotation associated with concussion, reflected in high strains as it is dynamically deformed. Therefore, through extensive characterization, we established a scaling approach to create similar mechanical loading of brain tissue between human TBI and the swine model. The parameters are based on Holbourn’s Scaling Equation [63], where the interaction of brain mass with the level of head rotational acceleration is taken into account [19, 39]. Specifically, for a swine brain of 90–100 g, the rotational acceleration forces must be increased eightfold or more to create the same tissue deformation that a human brain undergoes during concussion [41, 43]. This model recapitulates many aspects of the acute clinical presentation of mTBI, including loss of consciousness dependent on the angle of head rotation, as well as DAI in the absence of overt neuropathologies. However, there are anatomic differences between humans and swine, including skull architecture, that may affect the distribution of subtle neuropathologies and potentially outcome. In addition, the strain of swine used does not have nearly as prominent a falx cerebri as do humans. Since this structure may serve as a physical barrier during brain deformation, axonal pathology is much more prominent in midline structures in human TBI compared with the swine model.

Consistent with previous studies [44], here we identified DAI following a single rotational event in swine in a pattern and distribution consistent with mechanical deformation, and in the absence of any hemorrhage, brain swelling or ischemia. These findings support emerging clinical, neuroimaging and blood biomarker data indicating that DAI is a key pathological substrate of concussion in humans due to mechanical vulnerability of white matter axons

[12–14, 21, 43, 55, 59, 62, 80, 94, 95]. Nonetheless, these findings do not preclude the possibility that other brain structures also suffer mechanical damage within and beyond white matter.

Using this swine model, our current data also demonstrate that the brain vasculature is vulnerable to damage as a consequence of the mechanical forces of concussion. While the specific ultrastructural nature of this mechanical damage to vessels remains to be determined, the resulting abrupt disruption of BBB integrity is clearly evidenced by multifocal pathological extravasation of large serum proteins, FBG and IgG. Of note, FBG immunoreactivity was observed at all time points post-injury and was most marked with a survival duration of 6 h. Interestingly, a biphasic course of BBB dysfunction has previously been described in the acute phase following models of severe TBI in rodents [9, 10]. While our data trends towards a relative decrease in FBG immunoreactivity at 48 versus 72 h, a greater number of animals would be required to determine the time course of acute BBB opening. In addition, as the presence of serum proteins in brain parenchyma is determined both by their rate of extravasation and clearance, this is unlikely to be a precise measure of BBB opening at any given time-point. Future studies utilizing the terminal intravascular administration of exogenous labels, e.g. Evans blue, will be important to accurately determine the acute temporal time course of BBB leakage in this model.

The duration of BBB permeability in the swine model beyond the acute phase will also be important to explore. Indeed, considering that FBG extravasation has been observed in post-mortem human brain months and even years after a single moderate-severe TBI [34], a milder form of persisting BBB may also occur in some cases of concussion. While the resulting downstream pathological effects of BBB dysfunction remain to be determined in single concussion, BBB permeability along with perivascular neuropathologies including neurofibrillary and glial tauopathy have been reported in individuals with CTE following exposure to repetitive concussion [24, 56, 83].

In the present study, FBG and IgG immunoreactivity was observed in a stereotypical, multifocal distribution, typically surrounding vessels of variable size. Extravasated serum proteins were frequently present surrounding vessels at anatomical boundaries with juxtaposing material properties, including the gray–white interface, subpial cortex, and adjacent to the dentate gyrus and lateral ventricles. Moreover, while there was no difference in the overall extent of BBB leakage between hemispheres, stereotyped hemispheric differences in the distribution of extravasated serum proteins suggests BBB disruption occurs in a distribution consistent with a mechanical etiology.

To determine the clinical relevance of the findings in the swine concussion model, parallel examinations were performed on post-mortem tissue following human severe TBI. As expected, due to the differences in injury severity, far more extensive and widespread FBG extravasation was found in the human TBI cases than was observed in swine concussion. Nonetheless, there were notably similarities in the pattern of BBB disruption between the two species. As found in swine concussion, a multifocal distribution of FBG extravasation was apparent, with subpial vessels frequently affected and occasional focal disruptions at the gray–white boundary were also observed in the human cases. As with the findings in swine,

the location of these disruptions suggests a mechanical origin with a predominance at anatomic boundaries. Unlike the swine concussion model, however, there were additional changes typical of severe TBI in humans, including evolving hemorrhagic lesions, ischemic change and brain swelling. Moreover, human control brains also displayed some degree of serum protein extravasation, likely induced by protracted agonal or prolonged ischemic events around the time of death.

Following concussion in swine, within the white matter, there was considerable gross regional overlap of abnormal FBG immunoreactivity and axonal profiles accumulating APP. Specifically, approximately 60% of axons with an injured morphology were observed in regions with coincident FBG extravasation. This suggests that the overlapping pattern of both pathologies in white matter might reflect regions of higher mechanical injury during rotational acceleration. Since physical and computational models of swine TBI have shown both gray and white matter undergo a heterogeneous pattern of high stresses and strains, future studies could examine whether BBB disruption following *in vivo* injury could be used as a pathological marker for loading distribution throughout the entire brain.

The overlap of different neuropathologies agrees with biomechanics literature showing the mechanical threshold for compromise of the BBB overlaps with thresholds for axonal injury [8, 79]. In general, the direction of impact, acceleration profile, and relative size and shape of the brain all contribute to areas of maximum deformation within the brain during ‘real world’ impacts that cause concussion [22]. Thus, identification of BBB disruption may serve as a type of “injury strain gauge”, showing regions that endured the highest deformations in both the gray and white matter.

With regards to white matter, at the local scale, tissue deformations can parallel the trajectory of axons within a region, maximally stretching these axons. In this scenario, axonal injury may appear in the absence of BBB compromise. In comparison, if tissue stretch appears perpendicular to primary axonal pathways, axons are not stretched significantly and BBB compromise can occur prior to any evidence of axonal damage. Finally, when the local tissue deformation is enough to exceed both the local tolerance of the microvasculature and the tolerance of axons aligned with the deformation field, one would see the co-localization of BBB and axonal injury. We observed each of these three injury phenotypes in our swine concussion model. The process of accounting for the microanatomy of the brain in predicting injury risk is now appearing in computational models of the brain to predict concussion injury risk [29, 40, 64], and our observations reinforce the need to accurately align the biomechanical features of injury with the anatomy. In the future, we expect these computational efforts will evolve to include estimates of damage to the brain network structure [47], which would significantly enhance our ability to connect the initial injury to the consequences of the injury over time.

Intriguingly, in addition to leaking into the brain parenchyma, serum proteins were also found to be taken up by local cells. Perivascular clusters of both neurons and astrocytes immunoreactive for FBG and IgG were observed following both concussion in swine and severe TBI in humans. Similar cellular uptake of serum proteins, including FBG, has been described in other disorders where BBB dysfunction features, including cerebrovascular

disease [15, 90], epilepsy [53], multiple sclerosis [7, 45, 48], cerebral malaria [16], acquired immunodeficiency syndrome [65], HIV encephalitis [20] and Alzheimer's disease [72, 90, 92]. Surprisingly, there was minimal uptake of serum proteins by microglia when compared with astrocytes and neurons, which may reflect cell-specific uptake for the clearance of serum proteins after TBI. Notably, astrocytes have previously been demonstrated to selectively clear FBG in vitro [38]. Since neurons staining for FBG following concussion appeared morphologically normal at the time points examined in the present study, further temporal studies would be required to examine if this uptake has pathological consequences.

The specific mechanisms by which the extravasation of serum proteins in TBI are potentially neurotoxic remain to be explored. However, in addition to its role in hemostasis, FBG is increasingly recognized for its additional and diverse contribution to CNS pathology via mediation of inflammatory processes [4, 5], astrocyte activation [75] autoimmunity and demyelination [6, 73]. Moreover, FBG has been demonstrated to inhibit CNS neurite outgrowth in vitro and in vivo [74], and thus may be a potential barrier to axonal recovery in concussion, where white matter injury is a primary pathology [12–14, 21, 55, 59, 62, 80, 94, 95]. Interestingly, exposure of the brain to serum proteins has been speculated as a potential mechanism driving age-related tau astroglipathy (ARTAG), a pathological accumulation of abnormally phosphorylated tau in astrocytes that occurs in a subpial, subependymal and perivascular distribution [46]. However, the presence of ARTAG following TBI has yet to be characterized.

In addition to the exploration of potential downstream neuropathological consequences of serum protein extravasation, it will be critical to examine the pathophysiological mechanisms that drive BBB dysfunction in concussion. This may include the immediate mechanical failure of the barrier, potentially caused by direct disruption of endothelial tight-junctions. In contrast, downstream pathophysiological alterations to the BBB, including altered transcellular transport, will also be important to examine since it has been demonstrated following an impact model of TBI in cats [67]. Interestingly, the matrix metalloproteases (MMPs), including MMP-9 in particular, are increasingly recognized as mediators of BBB permeability following TBI and their role in concussion should also be determined [50, 60, 78, 96].

Overall, we demonstrate that acute BBB disruption is a primary consequence of head rotational acceleration in a swine model of concussion. This observation could help direct non-invasive diagnosis of concussion, such as advanced neuroimaging techniques to identify the extent and distribution of BBB leakage [91]. In addition, characterizing the nature and time course of BBB permeability may have direct relevance for the development of serum biomarkers for concussion [44, 81], and for the timing of delivery of potential pharmacological interventions.

Supplementary Material

Refer to Web version on PubMed Central for supplementary material.

Acknowledgments

The authors thank Kathryn Wofford for assistance with kinematic measurements. Research reported in this publication was supported by the Department of Defense Grant W81XWH-13-1-0052, and the *National Institute of Neurological Disorders and Stroke* of the National Institutes of Health under award numbers R01NS092398, R01NS094003 and R01NS038104, and the Department of Veterans Affairs under Merit Review number 101RX001097.

Ethical approval All applicable national, and institutional guidelines for the care and use of animals were followed. All procedures performed in studies involving animals were in accordance with the ethical standards of the institution or practice at which the studies were conducted.

References

- Adams JH, Doyle D, Ford I, Gennarelli TA, Graham DI, McLellan DR (1989) Diffuse axonal injury in head injury: definition, diagnosis and grading. *Histopathology* 15:49–59 [PubMed: 2767623]
- Adams JH, Graham DI, Gennarelli TA, Maxwell WL (1991) Diffuse axonal injury in non-missile head injury. *J Neurol Neurosurg Psychiatry* 54:481–483 [PubMed: 1880506]
- Adams JH, Graham DI, Murray LS, Scott G (1982) Diffuse axonal injury due to nonmissile head injury in humans: an analysis of 45 cases. *Ann Neurol* 12:557–563 [PubMed: 7159059]
- Adams RA, Bauer J, Flick MJ, Sikorski SL, Nuriel T, Lassmann H, Degen JL, Akassoglou K (2007) The fibrin-derived γ 377–395 peptide inhibits microglia activation and suppresses relapsing paralysis in central nervous system autoimmune disease. *J Exp Med* 204:571–582. 10.1084/jem.20061931 [PubMed: 17339406]
- Adams RA, Passino M, Sachs BD, Nuriel T, Akassoglou K (2004) Fibrin mechanisms and functions in nervous system pathology. *Mol Interv* 4:163–176. 10.1124/mi.4.3.6 [PubMed: 15210870]
- Akassoglou K, Adams RA, Bauer J, Mercado P, Tseveleki V, Lassmann H, Probert L, Strickland S (2004) Fibrin depletion decreases inflammation and delays the onset of demyelination in a tumor necrosis factor transgenic mouse model for multiple sclerosis. *Proc Natl Acad Sci USA* 101:6698–6703. 10.1073/pnas.0303859101 [PubMed: 15096619]
- Alvarez JI, Saint-Laurent O, Godschalk A, Terouz S, Briels C, Larouche S, Bourbonniere L, Larochelle C, Prat A (2015) Focal disturbances in the blood–brain barrier are associated with formation of neuroinflammatory lesions. *Neurobiol Dis* 74:14–24. 10.1016/j.nbd.2014.09.016 [PubMed: 25448765]
- Bain AC, Meaney DF (2000) Tissue-level thresholds for axonal damage in an experimental model of central nervous system white matter injury. *J Biomech Eng* 122:615–622 [PubMed: 11192383]
- Baldwin SA, Fugaccia I, Brown DR, Brown LV, Scheff SW (1996) Blood–brain barrier breach following cortical contusion in the rat. *J Neurosurg* 85:476–481. 10.3171/jns.1996.85.3.0476 [PubMed: 8751635]
- Barzo P, Marmarou A, Fatouros P, Corwin F, Dunbar J (1996) Magnetic resonance imaging—monitored acute blood–brain barrier changes in experimental traumatic brain injury. *J Neurosurg* 85:1113–1121. 10.3171/jns.1996.85.6.1113 [PubMed: 8929504]
- Bazarian JJ, McClung J, Shah MN, Cheng YT, Flesher W, Kraus J (2005) Mild traumatic brain injury in the United States, 1998–2000. *Brain Inj* 19:85–91 [PubMed: 15841752]
- Bazarian JJ, Zhong J, Blyth B, Zhu T, Kavcic V, Peterson D (2007) Diffusion tensor imaging detects clinically important axonal damage after mild traumatic brain injury: a pilot study. *J Neurotrauma* 24:1447–1459. 10.1089/neu.2007.0241 [PubMed: 17892407]
- Blumbergs PC, Scott G, Manavis J, Wainwright H, Simpson DA, McLean AJ (1994) Staining of amyloid precursor protein to study axonal damage in mild head injury. *Lancet* 344:1055–1056 [PubMed: 7523810]
- Blumbergs PC, Scott G, Manavis J, Wainwright H, Simpson DA, McLean AJ (1995) Topography of axonal injury as defined by amyloid precursor protein and the sector scoring method in mild and severe closed head injury. *J Neurotrauma* 12:565–572 [PubMed: 8683607]
- Bridges LR, Andoh J, Lawrence AJ, Khoong CH, Poon WW, Esiri MM, Markus HS, Hainsworth AH (2014) Blood–brain barrier dysfunction and cerebral small vessel disease (arteriolosclerosis)

- in brains of older people. *J Neuropathol Exp Neurol* 73:1026–1033. 10.1097/NEN.000000000000124 [PubMed: 25289893]
16. Brown H, Hien TT, Day N, Mai NT, Chuong LV, Chau TT, Loc PP, Phu NH, Bethell D, Farrar J et al. (1999) Evidence of blood–brain barrier dysfunction in human cerebral malaria. *Neuropathol Appl Neurobiol* 25:331–340 [PubMed: 10476050]
 17. Browne KD, Chen XH, Meaney DF, Smith DH (2011) Mild traumatic brain injury and diffuse axonal injury in swine. *J Neurotrauma* 28:1747–1755. 10.1089/neu.2011.1913 [PubMed: 21740133]
 18. Coronado VG, Haileyesus T, Cheng TA, Bell JM, Haarbauer-Krupa J, Lionbarger MR, Flores-Herrera J, McGuire LC, Gilchrist J (2015) Trends in sports- and recreation-related traumatic brain injuries treated in US emergency departments: the National Electronic Injury Surveillance System-All Injury Program (NEISS-AIP) 2001–2012. *J Head Trauma Rehabil* 30:185–197. 10.1097/HTR.000000000000156 [PubMed: 25955705]
 19. Cullen DK, Harris JP, Browne KD, Wolf JA, Duda JE, Meaney DF, Margulies SS, Smith DH (2016) A porcine model of traumatic brain injury via head rotational acceleration. *Methods Mol Biol* 1462:289–324. 10.1007/978-1-4939-3816-2_17 [PubMed: 27604725]
 20. Dallasta LM, Pisarov LA, Esplen JE, Werley JV, Moses AV, Nelson JA, Achim CL (1999) Blood–brain barrier tight junction disruption in human immunodeficiency virus-1 encephalitis. *Am J Pathol* 155:1915–1927. 10.1016/S0002-9440(10)65511-3 [PubMed: 10595922]
 21. Eierud C, Craddock RC, Fletcher S, Aulakh M, King-Casas B, Kuehl D, LaConte SM (2014) Neuroimaging after mild traumatic brain injury: review and meta-analysis. *NeuroImage Clin* 4:283–294. 10.1016/j.nicl.2013.12.009 [PubMed: 25061565]
 22. Gabler LF, Crandall JR, Panzer MB (2016) Assessment of kinematic brain injury metrics for predicting strain responses in diverse automotive impact conditions. *Ann Biomed Eng* 44:3705–3718. 10.1007/s10439-016-1697-0 [PubMed: 27436295]
 23. Geddes JF, Vowles GH, Beer TW, Ellison DW (1997) The diagnosis of diffuse axonal injury: implications for forensic practice. *Neuropathol Appl Neurobiol* 23:339–347 [PubMed: 9292874]
 24. Geddes JF, Vowles GH, Nicoll JA, Revesz T (1999) Neuronal cytoskeletal changes are an early consequence of repetitive head injury. *Acta Neuropathol* 98:171–178 [PubMed: 10442557]
 25. Geddes JF, Whitwell HL, Graham DI (2000) Traumatic axonal injury: practical issues for diagnosis in medicolegal cases. *Neuropathol Appl Neurobiol* 26:105–116 [PubMed: 10840273]
 26. Gennarelli TA, Thibault LE, Adams JH, Graham DI, Thompson CJ, Marcincin RP (1982) Diffuse axonal injury and traumatic coma in the primate. *Ann Neurol* 12:564–574. 10.1002/ana.410120611 [PubMed: 7159060]
 27. Gentleman SM, Nash MJ, Sweeting CJ, Graham DI, Roberts GW (1993) Beta-amyloid precursor protein (beta APP) as a marker for axonal injury after head injury. *Neurosci Lett* 160:139–144 [PubMed: 8247344]
 28. Gentleman SM, Roberts GW, Gennarelli TA, Maxwell WL, Adams JH, Kerr S, Graham DI (1995) Axonal injury: a universal consequence of fatal closed head injury? *Acta Neuropathol* 89:537–543 [PubMed: 7676809]
 29. Giordano C, Kleiven S (2014) Evaluation of axonal strain as a predictor for mild traumatic brain injuries using finite element modeling. *Stapp Car Crash J* 58:29–61 [PubMed: 26192949]
 30. Graham DI, Gennarelli TA, McIntosh TK (2002) *Greenfield's neuropathology*. Arnold, London, UK
 31. Graham DI, Gentleman SM, Lynch A, Roberts GW (1995) Distribution of beta-amyloid protein in the brain following severe head injury. *Neuropathol Appl Neurobiol* 21:27–34 [PubMed: 7770117]
 32. Graham DI, Smith C, Reichard R, Leclercq PD, Gentleman SM (2004) Trials and tribulations of using beta-amyloid precursor protein immunohistochemistry to evaluate traumatic brain injury in adults. *Forensic Sci Int* 146:89–96. 10.1016/S0379-0738(03)00274-3 [PubMed: 15542268]
 33. Hay J, Johnson VE, Smith DH, Stewart W (2016) Chronic traumatic encephalopathy: the neuropathological legacy of traumatic brain injury. *Annu Rev Pathol* 11:21–45. 10.1146/annurev-pathol-012615-044116 [PubMed: 26772317]

34. Hay JR, Johnson VE, Young AM, Smith DH, Stewart W (2015) Blood–brain barrier disruption is an early event that may persist for many years after traumatic brain injury in humans. *J Neuropathol Exp Neurol* 74:1147–1157. 10.1097/NEN.0000000000000261 [PubMed: 26574669]
35. Hayashi T, Ago K, Ago M, Ogata M (2009) Two patterns of beta-amyloid precursor protein (APP) immunoreactivity in cases of blunt head injury. *Leg Med (Tokyo)* 11(Suppl 1):S171–S173. 10.1016/j.legalmed.2009.01.076 [PubMed: 19251455]
36. Holbourn AHS (1945) Mechanics of brain injuries. *Br Med Bull* 3:147–149
37. Holbourn AHS (1943) Mechanics of head injury. *Lancet* 242:438–441
38. Hsiao TW, Swarup VP, Kuberan B, Tresco PA, Hlady V (2013) Astrocytes specifically remove surface-adsorbed fibrinogen and locally express chondroitin sulfate proteoglycans. *Acta Biomater* 9:7200–7208. 10.1016/j.actbio.2013.02.047 [PubMed: 23499985]
39. Ibrahim NG, Natesh R, Szczesny SE, Ryall K, Eucker SA, Coats B, Margulies SS (2010) In situ deformations in the immature brain during rapid rotations. *J Biomech Eng* 132:044501 10.1115/1.4000956 [PubMed: 20387974]
40. Ji S, Zhao W, Ford JC, Beckwith JG, Bolander RP, Greenwald RM, Flashman LA, Paulsen KD, McAllister TW (2015) Groupwise evaluation and comparison of white matter fiber strain and maximum principal strain in sports-related concussion. *J Neurotrauma* 32:441–454. 10.1089/neu.2013.3268 [PubMed: 24735430]
41. Johnson VE, Meaney DF, Cullen DK, Smith DH (2015) Animal models of traumatic brain injury. *Handb Clin Neurol* 127:115–128. 10.1016/B978-0-444-52892-6.00008-8 [PubMed: 25702213]
42. Johnson VE, Stewart JE, Begbie FD, Trojanowski JQ, Smith DH, Stewart W (2013) Inflammation and white matter degeneration persist for years after a single traumatic brain injury. *Brain* 136:28–42 [PubMed: 23365092]
43. Johnson VE, Stewart W, Smith DH (2013) Axonal pathology in traumatic brain injury. *Exp Neurol* 246:35–43. 10.1016/j.expneurol.2012.01.013 [PubMed: 22285252]
44. Johnson VE, Stewart W, Weber MT, Cullen DK, Siman R, Smith DH (2016) SNTF immunostaining reveals previously undetected axonal pathology in traumatic brain injury. *Acta Neuropathol* 131:115–135. 10.1007/s00401-015-1506-0 [PubMed: 26589592]
45. Kirk J, Plumb J, Mirakhur M, McQuaid S (2003) Tight junctional abnormality in multiple sclerosis white matter affects all calibres of vessel and is associated with blood–brain barrier leakage and active demyelination. *J Pathol* 201:319–327. 10.1002/path.1434 [PubMed: 14517850]
46. Kovacs GG, Robinson JL, Xie SX, Lee EB, Grossman M, Wolk DA, Irwin DJ, Weintraub D, Kim CF, Schuck T et al. (2017) Evaluating the patterns of aging-related tau astroglial pathology unravels novel insights into brain aging and neurodegenerative diseases. *J Neuropathol Exp Neurol* 76:270–288. 10.1093/jnen/nlx007 [PubMed: 28340083]
47. Kraft RH, McKee PJ, Dagro AM, Grafton ST (2012) Combining the finite element method with structural connectome-based analysis for modeling neurotrauma: connectome neurotrauma mechanics. *PLoS Comput Biol* 8:e1002619 10.1371/journal.pcbi.1002619 [PubMed: 22915997]
48. Kwon EE, Prineas JW (1994) Blood–brain barrier abnormalities in longstanding multiple sclerosis lesions. An immunohistochemical study. *J Neuropathol Exp Neurol* 53:625–636 [PubMed: 7964903]
49. Leclercq PD, McKenzie JE, Graham DI, Gentleman SM (2001) Axonal injury is accentuated in the caudal corpus callosum of head-injured patients. *J Neurotrauma* 18:1–9 [PubMed: 11200244]
50. Lee P, Kim J, Williams R, Sandhir R, Gregory E, Brooks WM, Berman NE (2012) Effects of aging on blood–brain barrier and matrix metalloproteases following controlled cortical impact in mice. *Exp Neurol* 234:50–61. 10.1016/j.expneurol.2011.12.016 [PubMed: 22201549]
51. Levin HS, Diaz-Arrastia RR (2015) Diagnosis, prognosis, and clinical management of mild traumatic brain injury. *Lancet Neurol* 14:506–517. 10.1016/S1474-4422(15)00002-2 [PubMed: 25801547]
52. Liu HM, Atack JR, Rapoport SI (1989) Immunohistochemical localization of intracellular plasma proteins in the human central nervous system. *Acta Neuropathol* 78:16–21 [PubMed: 2735186]
53. Liu JY, Thom M, Catarino CB, Martinian L, Figarella-Branger D, Bartolomei F, Koeppe M, Sisodiya SM (2012) Neuropathology of the blood–brain barrier and pharmaco-resistance in human epilepsies. *Brain* 135:3115–3133. 10.1093/brain/aws147 [PubMed: 22750659]

54. Margulies SS, Thibault LE, Gennarelli TA (1990) Physical model simulations of brain injury in the primate. *J Biomech* 23:823–836. 10.1016/0021-9290(90)90029-3 [PubMed: 2384494]
55. Mayer AR, Ling J, Mannell MV, Gasparovic C, Phillips JP, Doezema D, Reichard R, Yeo RA (2010) A prospective diffusion tensor imaging study in mild traumatic brain injury. *Neurology* 74:643–650. 10.1212/WNL.0b013e3181d0ccdd [PubMed: 20089939]
56. McKee AC, Cairns NJ, Dickson DW, Folkerth RD, Keene CD, Litvan I, Perl DP, Stein TD, Vonsattel JP, Stewart W et al. (2016) The first NINDS/NIBIB consensus meeting to define neuropathological criteria for the diagnosis of chronic traumatic encephalopathy. *Acta Neuropathol* 131:75–86. 10.1007/s00401-015-1515-z [PubMed: 26667418]
57. McKee AC, Stein TD, Nowinski CJ, Stern RA, Daneshvar DH, Alvarez VE, Lee HS, Hall G, Wojtowicz SM, Baugh CM et al. (2013) The spectrum of disease in chronic traumatic encephalopathy. *Brain* 136:43–64. 10.1093/brain/aws307 [PubMed: 23208308]
58. Meaney DF, Smith DH, Shreiber DI, Bain AC, Miller RT, Ross DT, Gennarelli TA (1995) Biomechanical analysis of experimental diffuse axonal injury. *J Neurotrauma* 12:689–694 [PubMed: 8683620]
59. Miles L, Grossman RI, Johnson G, Babb JS, Diller L, Inglese M (2008) Short-term DTI predictors of cognitive dysfunction in mild traumatic brain injury. *Brain Inj* 22:115–122. 10.1080/02699050801888816 [PubMed: 18240040]
60. Mori T, Wang X, Aoki T, Lo EH (2002) Downregulation of matrix metalloproteinase-9 and attenuation of edema via inhibition of ERK mitogen activated protein kinase in traumatic brain injury. *J Neurotrauma* 19:1411–1419. 10.1089/089771502320914642 [PubMed: 12490006]
61. Nguyen R, Fiest KM, McChesney J, Kwon CS, Jette N, Frolkis AD, Atta C, Mah S, Dhaliwal H, Reid A et al. (2016) The international incidence of traumatic brain injury: a systematic review and meta-analysis. *Can J Neurol Sci* 43:774–785. 10.1017/cjn.2016.290 [PubMed: 27670907]
62. Niogi SN, Mukherjee P, Ghajar J, Johnson C, Kolster RA, Sarkar R, Lee H, Meeker M, Zimmerman RD, Manley GT et al. (2008) Extent of microstructural white matter injury in postconcussive syndrome correlates with impaired cognitive reaction time: a 3T diffusion tensor imaging study of mild traumatic brain injury. *AJNR Am J Neuroradiol* 29:967–973. 10.3174/ajnr.A0970 [PubMed: 18272556]
63. Ommaya AK, Yarnell P, Hirsch AE, Harris EH (1967) Scaling of experimental data on cerebral concussion in sub-human primates to concussive thresholds in man. SAE Technical Paper. In: proceedings of the 11th Stapp car crash conference, Warrendale, PA, pp 73–80
64. Patton DA, McIntosh AS, Kleiven S (2015) The biomechanical determinants of concussion: finite element simulations to investigate tissue-level predictors of injury during sporting impacts to the unprotected head. *J Appl Biomech* 31:264–268. 10.1123/jab.2014-0223 [PubMed: 25781376]
65. Petito CK, Cash KS (1992) Blood–brain barrier abnormalities in the acquired immunodeficiency syndrome: immunohistochemical localization of serum proteins in postmortem brain. *Ann Neurol* 32:658–666. 10.1002/ana.410320509 [PubMed: 1449246]
66. Povlishock JT, Becker DP, Miller JD, Jenkins LW, Dietrich WD (1979) The morphopathologic substrates of concussion? *Acta Neuropathol* 47:1–11 [PubMed: 463502]
67. Povlishock JT, Becker DP, Sullivan HG, Miller JD (1978) Vascular permeability alterations to horseradish peroxidase in experimental brain injury. *Brain Res* 153:223–239 [PubMed: 687980]
68. Rabinowitz AR, Li X, McCauley SR, Wilde EA, Barnes A, Hanten G, Mendez D, McCarthy JJ, Levin HS (2015) Prevalence and predictors of poor recovery from mild traumatic brain injury. *J Neurotrauma* 32:1488–1496. 10.1089/neu.2014.3555 [PubMed: 25970233]
69. Reichard RR, Smith C, Graham DI (2005) The significance of beta-APP immunoreactivity in forensic practice. *Neuropathol Appl Neurobiol* 31:304–313. 10.1111/j.1365-2990.2005.00645.x [PubMed: 15885067]
70. Roe C, Sveen U, Alvsaker K, Bautz-Holter E (2009) Post-concussion symptoms after mild traumatic brain injury: influence of demographic factors and injury severity in a 1-year cohort study. *Disabil Rehabil* 31:1235–1243. 10.1080/09638280802532720 [PubMed: 19116810]
71. Ross DT, Meaney DF, Sabol MK, Smith DH, Gennarelli TA (1994) Distribution of forebrain diffuse axonal injury following inertial closed head injury in miniature swine. *Exp Neurol* 126:291–299. 10.1006/exnr.1994.1067 [PubMed: 7925827]

72. Ryu JK, McLarnon JG (2009) A leaky blood-brain barrier, fibrinogen infiltration and microglial reactivity in inflamed Alzheimer's disease brain. *J Cell Mol Med* 13:2911–2925. 10.1111/j.1582-4934.2008.00434.x [PubMed: 18657226]
73. Ryu JK, Petersen MA, Murray SG, Baeten KM, Meyer-Franke A, Chan JP, Vagena E, Bedard C, Machado MR, Rios Coronado PE et al. (2015) Blood coagulation protein fibrinogen promotes autoimmunity and demyelination via chemokine release and antigen presentation. *Nat Commun* 6:8164 10.1038/ncomms9164 [PubMed: 26353940]
74. Schachtrup C, Lu P, Jones LL, Lee JK, Lu J, Sachs BD, Zheng B, Akassoglou K (2007) Fibrinogen inhibits neurite outgrowth via beta 3 integrin-mediated phosphorylation of the EGF receptor. *Proc Natl Acad Sci USA* 104:11814–11819. 10.1073/pnas.0704045104 [PubMed: 17606926]
75. Schachtrup C, Ryu JK, Helmrück MJ, Vagena E, Galanakis DK, Degen JL, Margolis RU, Akassoglou K (2010) Fibrinogen triggers astrocyte scar formation by promoting the availability of active TGF-beta after vascular damage. *J Neurosci* 30:5843–5854. 10.1523/JNEUROSCI.0137-10.2010 [PubMed: 20427645]
76. Shahim P, Tegner Y, Wilson DH, Randall J, Skillback T, Pazooki D, Kallberg B, Blennow K, Zetterberg H (2014) Blood biomarkers for brain injury in concussed professional ice hockey players. *JAMA Neurol* 71:684–692. 10.1001/jamaneurol.2014.367 [PubMed: 24627036]
77. Sherriff FE, Bridges LR, Sivaloganathan S (1994) Early detection of axonal injury after human head trauma using immunocytochemistry for beta-amyloid precursor protein. *Acta Neuropathol (Berl)* 87:55–62 [PubMed: 8140894]
78. Shigemori Y, Katayama Y, Mori T, Maeda T, Kawamata T (2006) Matrix metalloproteinase-9 is associated with blood-brain barrier opening and brain edema formation after cortical contusion in rats. *Acta Neurochir Suppl* 96:130–133 [PubMed: 16671440]
79. Shreiber D, Bain A, Meaney D (1997) In vivo thresholds for mechanical injury to the blood-brain barrier. *SAE Technical Paper* 973335. 10.4271/973335
80. Siman R, Giovannone N, Hanten G, Wilde EA, McCauley SR, Hunter JV, Li X, Levin HS, Smith DH (2013) Evidence that the blood biomarker SNTF predicts brain imaging changes and persistent cognitive dysfunction in mild TBI patients. *Front Neurol* 4:190 10.3389/fneur.2013.00190 [PubMed: 24302918]
81. Siman R, Shahim P, Tegner Y, Blennow K, Zetterberg H, Smith DH (2015) Serum SNTF increases in concussed professional ice hockey players and relates to the severity of postconcussion symptoms. *J Neurotrauma*. 10.1089/neu.2014.3698 (in press)
82. Smith DH, Chen XH, Xu BN, McIntosh TK, Gennarelli TA, Meaney DF (1997) Characterization of diffuse axonal pathology and selective hippocampal damage following inertial brain trauma in the pig. *J Neuropathol Exp Neurol* 56:822–834 [PubMed: 9210879]
83. Smith DH, Johnson VE, Stewart W (2013) Chronic neuropathologies of single and repetitive TBI: substrates of dementia? *Nat Rev Neurol* 9:211–221 [PubMed: 23458973]
84. Smith DH, Meaney DF (2000) Axonal damage in traumatic brain injury. *Neuroscientist* 6:483–495
85. Smith DH, Nonaka M, Miller R, Leoni M, Chen XH, Alsop D, Meaney DF (2000) Immediate coma following inertial brain injury dependent on axonal damage in the brainstem. *J Neurosurg* 93:315–322. 10.3171/jns.2000.93.2.0315 [PubMed: 10930019]
86. Smith DH, Wolf JA, Lusardi TA, Lee VM, Meaney DF (1999) High tolerance and delayed elastic response of cultured axons to dynamic stretch injury. *J Neurosci* 19:4263–4269 [PubMed: 10341230]
87. Strich SJ (1961) Sharing of the nerve fibers as a cause of brain damage due to head injury: a pathological study of 20 cases. *Lancet* 278:443–448
88. Tang-Schomer MD, Johnson VE, Baas PW, Stewart W, Smith DH (2012) Partial interruption of axonal transport due to microtubule breakage accounts for the formation of periodic varicosities after traumatic axonal injury. *Exp Neurol* 233:364–372. 10.1016/j.expneurol.2011.10.030 [PubMed: 22079153]
89. Thibault L, Gennarelli TA, Margulies SS, et al. (1990) The strain dependent pathophysiological consequences of inertial loading on central nervous system tissue. In: proceedings of the international conference on the Biomechanics Of Impact Lyon, France, pp 191–202

90. Tomimoto H, Akiguchi I, Suenaga T, Nishimura M, Wakita H, Nakamura S, Kimura J (1996) Alterations of the blood–brain barrier and glial cells in white-matter lesions in cerebrovascular and Alzheimer’s disease patients. *Stroke* 27:2069–2074 [PubMed: 8898818]
91. Veksler R, Shelef I, Friedman A (2014) Blood–brain barrier imaging in human neuropathologies. *Arch Med Res* 45:646–652. 10.1016/j.arcmed.2014.11.016 [PubMed: 25453223]
92. Viggars AP, Wharton SB, Simpson JE, Matthews FE, Brayne C, Savva GM, Garwood C, Drew D, Shaw PJ, Ince PG (2011) Alterations in the blood–brain barrier in ageing cerebral cortex in relationship to Alzheimer-type pathology: a study in the MRC-CFAS population neuropathology cohort. *Neurosci Lett* 505:25–30. 10.1016/j.neulet.2011.09.049 [PubMed: 21970975]
93. Weissberg I, Veksler R, Kamintsky L, Saar-Ashkenazy R, Milikovsky DZ, Shelef I, Friedman A (2014) Imaging blood–brain barrier dysfunction in football players. *JAMA Neurol* 71:1453–1455. 10.1001/jamaneurol.2014.2682 [PubMed: 25383774]
94. Wilde EA, McCauley SR, Hunter JV, Bigler ED, Chu Z, Wang ZJ, Hanten GR, Troyanskaya M, Yallampalli R, Li X et al. (2008) Diffusion tensor imaging of acute mild traumatic brain injury in adolescents. *Neurology* 70:948–955. 10.1212/01.wnl.0000305961.68029.54 [PubMed: 18347317]
95. Yallampalli R, Wilde EA, Bigler ED, McCauley SR, Hanten G, Troyanskaya M, Hunter JV, Chu Z, Li X, Levin HS (2013) Acute white matter differences in the fornix following mild traumatic brain injury using diffusion tensor imaging. *J Neuroimaging Off J Am Soc Neuroimaging* 23:224–227. 10.1111/j.1552-6569.2010.00537.x
96. Zhang H, Adwanikar H, Werb Z, Noble-Haeusslein LJ (2010) Matrix metalloproteinases and neurotrauma: evolving roles in injury and reparative processes. *Neuroscientist* 16:156–170. 10.1177/1073858409355830 [PubMed: 20400713]

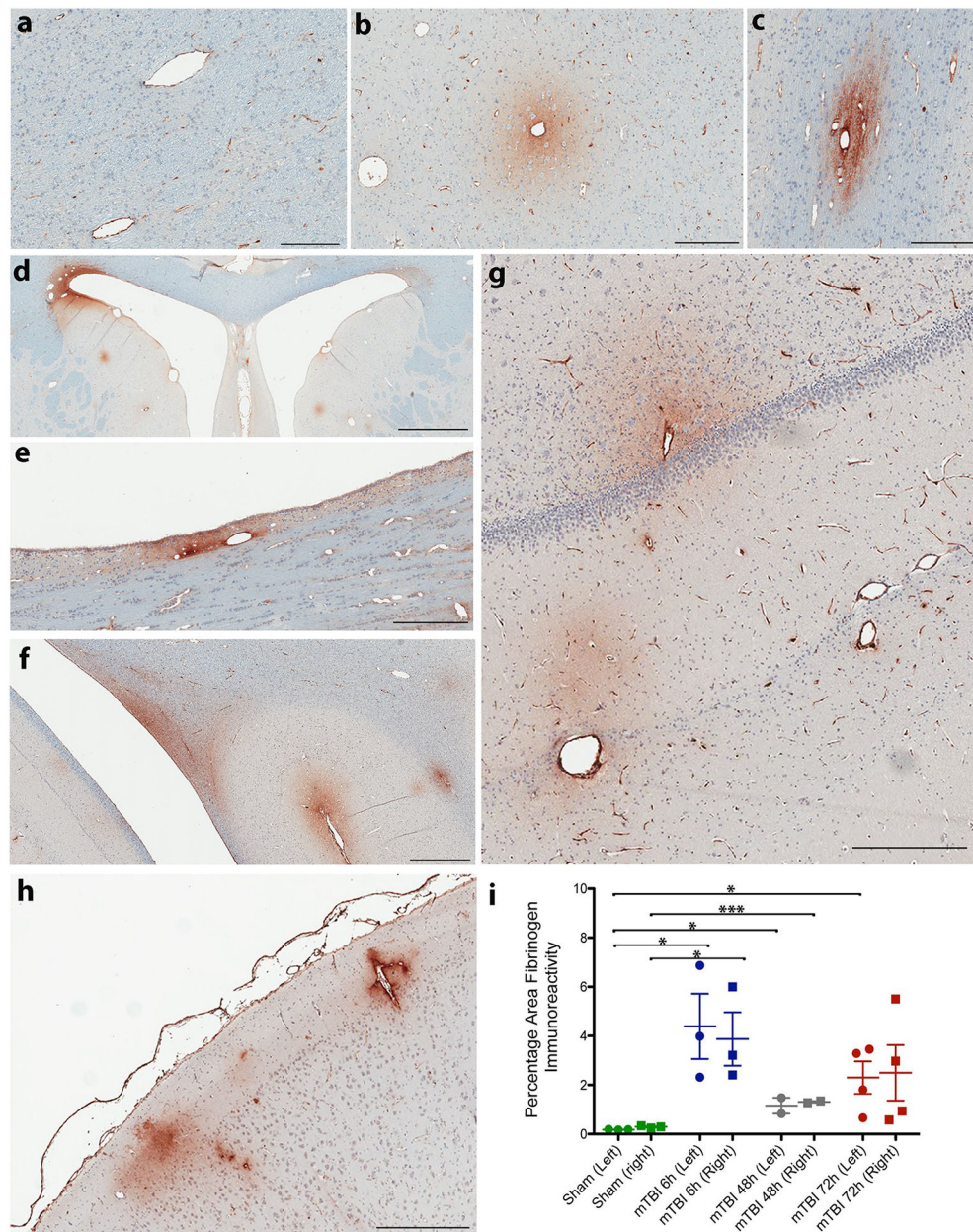


Fig. 1.

Experimental concussion induces multifocal BBB leakage. **a** An absence of FBG immunoreactivity in the subcortical white matter in a sham animal. Immunoreactivity specific for FBG; **b** surrounding a vessel in the parenchyma of the thalamus 6 h following a single experimental concussion; **c** in the subcortical white matter at the level of the head of the caudate nucleus 48 h following experimental concussion; **d** at the tip of the lateral ventricle preferentially in left hemisphere (leading hemisphere in rotation) 6 h following experimental concussion; **e** at the ventricular interface of the corpus callosum 72 h following experimental concussion; **f** in the periventricular white matter and depth of the sulci at the lateral aspect of the parahippocampal cortex where it meets the inferior temporal gyrus, 6 h post-experimental concussion; **g** adjacent to the dentate gyrus and vessels of the

hippocampal fissure 6 h following experimental concussion; and **h** at the cortical surface in the frontal lobe 72 h post-experimental concussion. **i** Graph showing the percentage area of FBG immunoreactivity for the whole coronal brain hemispheres for each animal in all 5 levels combined. Scale bars **a, c** 200 μm , **b, e** 300 μm , **d** 3 mm, **f** 2 mm, **g** 400 μm , **h** 500 μm

Author Manuscript

Author Manuscript

Author Manuscript

Author Manuscript

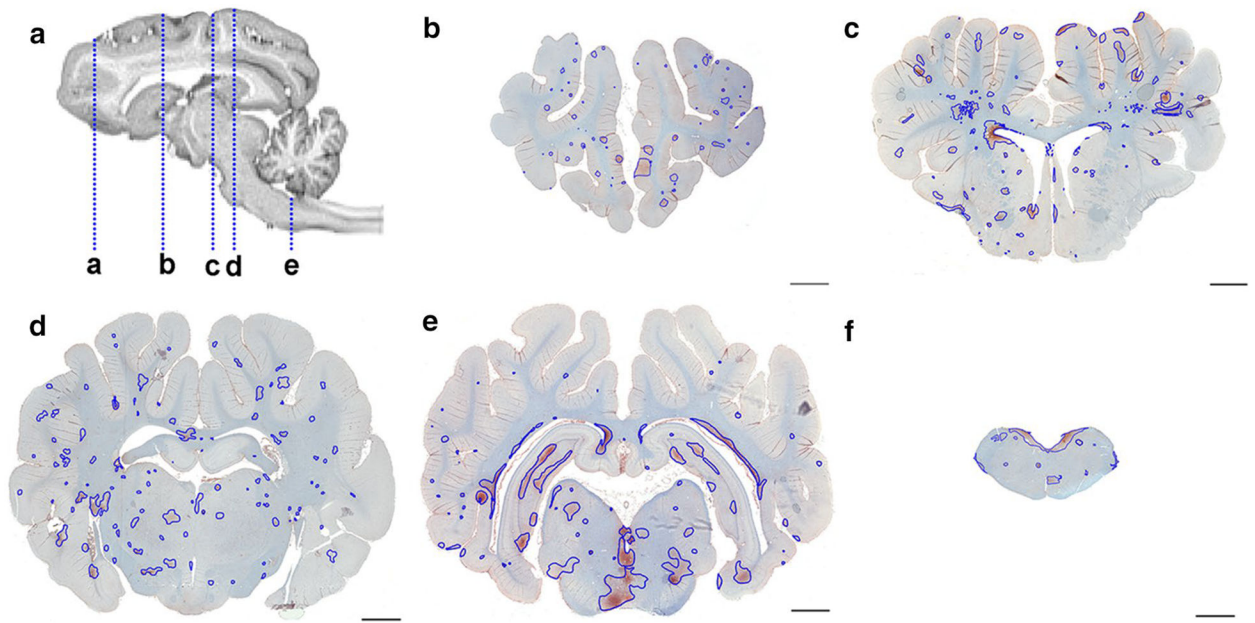


Fig. 2. BBB leakage occurs in a biomechanical distribution after experimental concussion. **a** MRI image with vertical dotted lines indicating the levels of brain examined in the coronal plane. **b–f** Whole brain coronal maps showing FBG extravasation annotated manually following high resolution digital scanning in each of the 5 levels denoted in **a**. Scale bars 5 mm

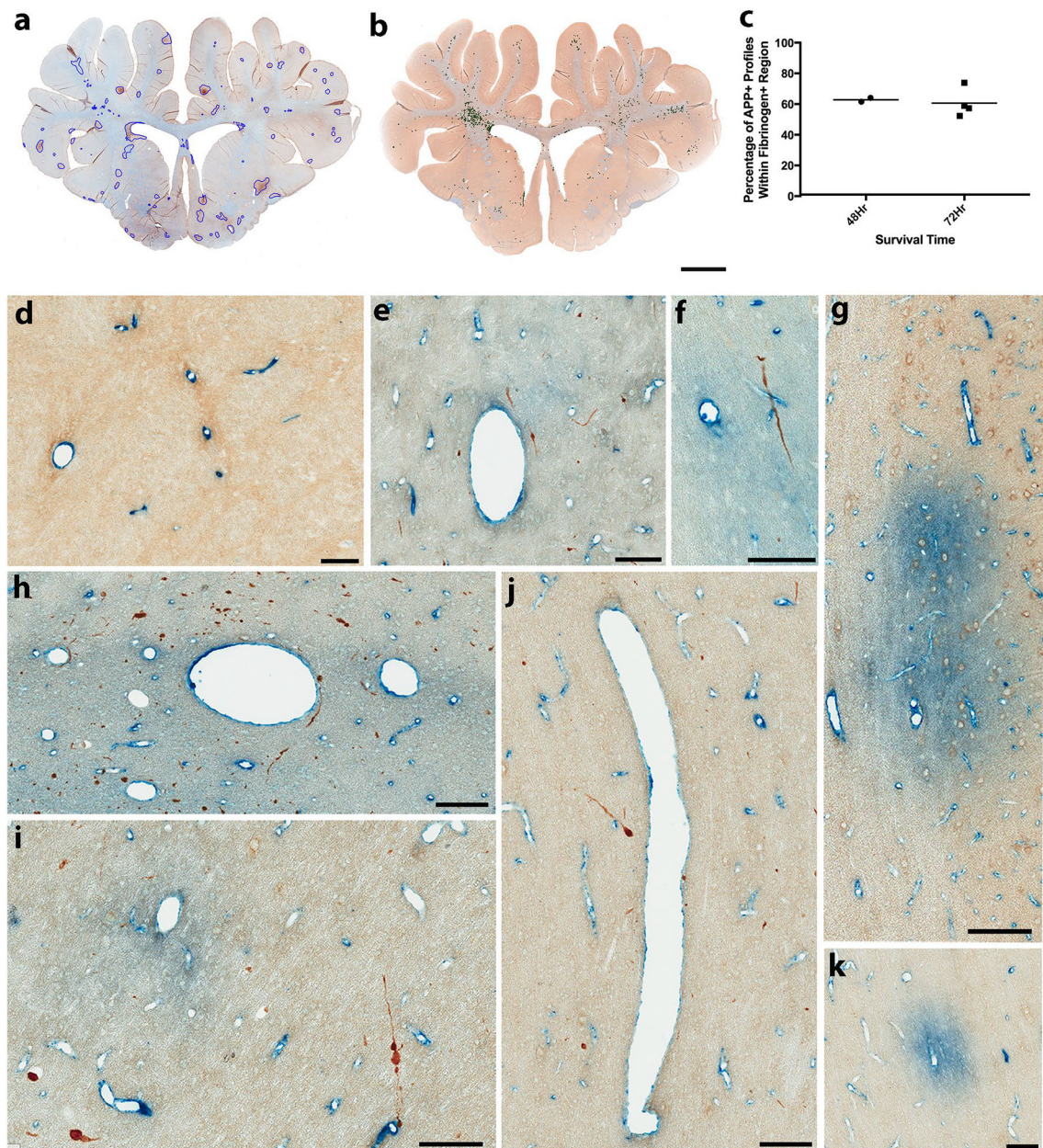


Fig. 3. BBB leakage has limited regional overlap with axonal pathology after experimental concussion. **a** Whole section map of annotated FBG immunoreactivity at 48 h post-experimental concussion. **b** Adjacent section to **a** showing APP positive axonal pathology in a distribution that overlaps with FBG leakage in the white matter. **c** Graph showing the percentage of APP positive profiles identified in regions where coincident FBG extravasation is observed via multiple chromagen staining at 48 and 72 h post-experimental concussion. **d** FBG (blue) confined to the vascular compartment in a sham with no extravasation into the brain parenchyma. No axonal pathology is observed (brown). **e, f, h** Regions of extensive FBG extravasation (blue) and axonal pathology (brown) in the **e** deep cortical white matter 48 h following experimental concussion, **f** gray–white interface of the

frontal cortex at 72 h post-experimental concussion and **h** the periventricular region of the leading hemisphere at 48 h post-experimental concussion. **i** Scattered axonal pathology both within and beyond regions of extravasated FBG in the white matter at 48 h postexperimental concussion. **j** APP immunoreactive axonal pathology in the perivascular region without FBG extravasation. **g, k** Overt FBG extravasation without axonal pathology in the gray–white interface (**g**) and deep white matter (**k**) at 48 h post-experimental concussion. Scale bars **a, b** 6 mm, **d–k** 100 μ m

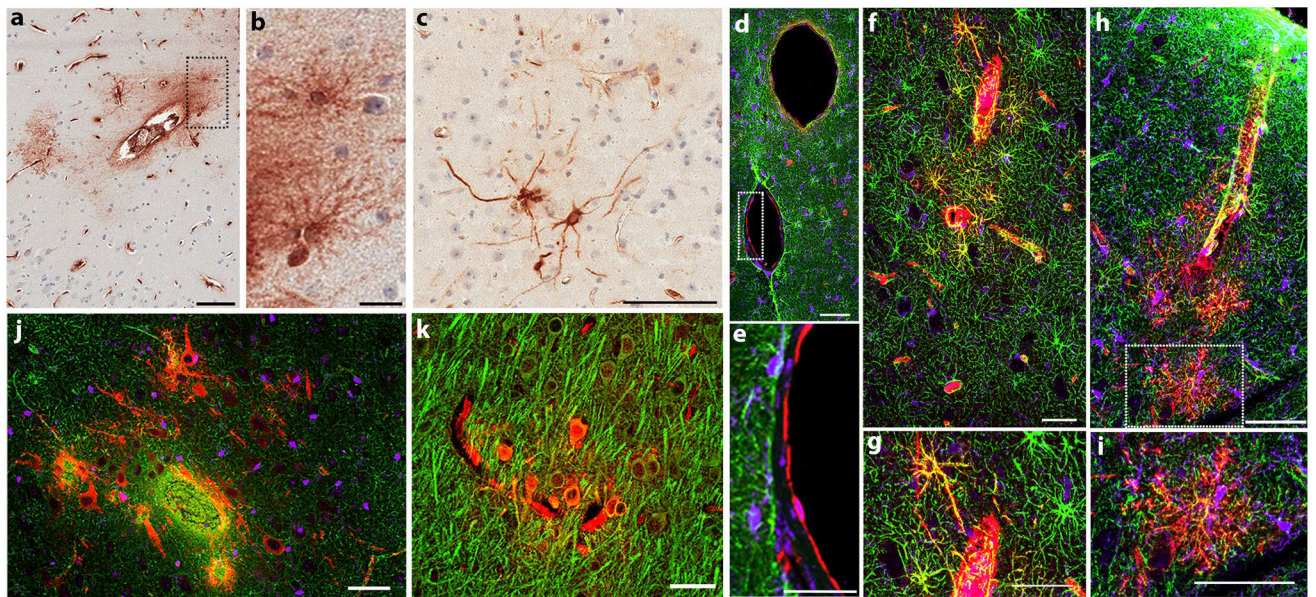


Fig. 4. Astrocytes and neurons internalize blood-borne proteins after experimental concussion. **a** FBG immunoreactive cells with a glial morphology at the depth of the sulcus within the inferior temporal gyrus 48 h post-experimental concussion. **b** Higher magnification of box in **a**. **c** Cells with neuronal morphology and immunoreactive for FBG in the caudate nucleus 72 h post-experimental concussion. **d** Normal vessels without FBG (red) extravasation. FBG is confined to the vessel lumen without co-localization with astrocytes (GFAP; green) or microglia (IBA-1; purple). **e** Higher magnification of box in **d**. **f** Vessels in premotor cortex showing marked FBG (red) extravasation 72 h post-experimental concussion. Co-localization with astrocytes (GFAP; green) is observed. Only minimal co-localization with microglia (IBA-1; purple) was observed in cells immediately adjacent to the vessel. **g** Higher magnification of region in **f**. **h** Penetrating surface vessels of parietal cortex showing marked FBG (red) extravasation 72 h post-experimental concussion with co-localization with astrocytes (GFAP; green). **i** Higher magnification of box in **h**. **j** Cells in the frontal cortex with neuronal morphology that are negative for IBA-1 (purple) and GFAP (green), yet co-localize with FBG (red). **k** Neuronal cell-type was confirmed with evidence of co-localization of MAP-2 (green) cells and FBG (red). Scale bars **a, c** 100 μm , **b, e** 25 μm , **d, f–k** 50 μm

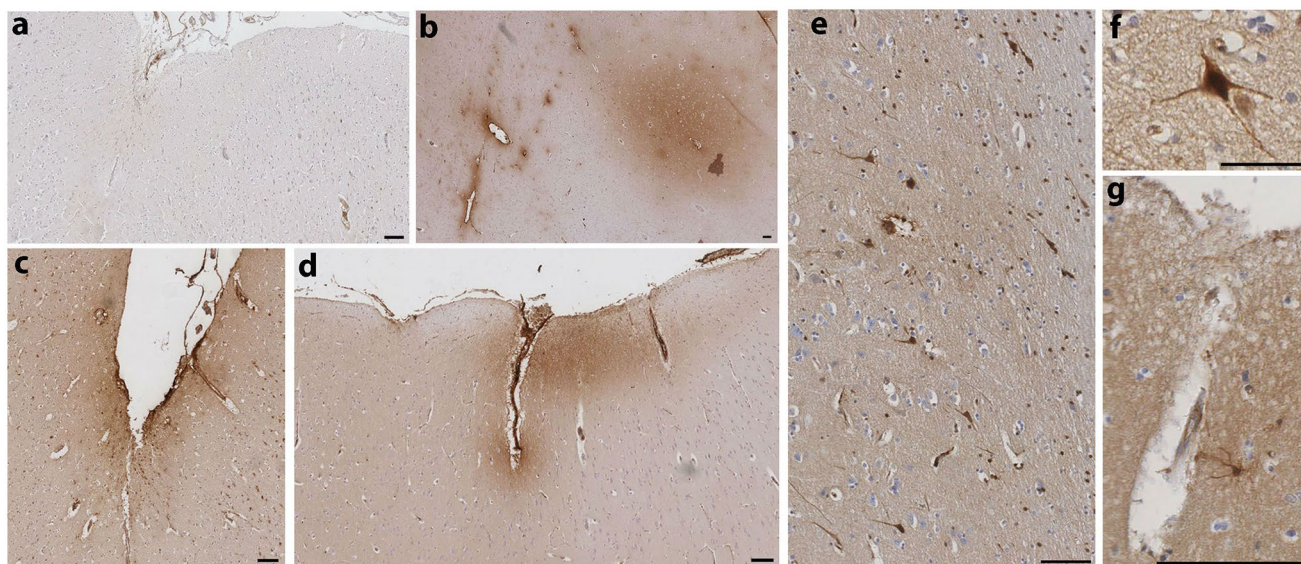


Fig. 5.

FBG extravasation after acute severe TBI in humans. **a** An absence of FBG immunoreactivity out with the vascular compartment in a 20-year-old male control that died following a sudden cardiac event secondary to hypertrophic cardiomyopathy. **b** Marked FBG extravasation in a perivascular distribution at the gray–white interface in the superior frontal gyri in a 20-year-old male 48 h following TBI caused by assault. **c** FBG extravasation and associated glial uptake at the depth of sulci in a 58-year-old male that died 6 h following TBI caused by assault. **d** A penetrating vessel at the cortical surface of the cingulate gyrus surrounded by extravasated FBG (same case as **b**). **e** Extensive neuronal uptake of FBG in the superior frontal gyrus in a 58-year-old male 6 h after TBI caused by a fall. **f** High magnification of a neuron immunoreactive for FBG in an 18-year-old male 10 h after a fall. **g** An astrocyte immunoreactive for FBG with process extending towards a vessel at the surface of the cingulate cortex in a 56-year-old female 24 h following TBI caused by a road traffic accident. Scale bars **a–e, g** 100 μm , **f** 50 μm

Table 1

Demographic and clinical data

	TBI cases (n = 12)	Controls (n = 7)
Age	Mean (range) 44 years (18–58 years)	32 years (16–60 years)
Males	7 (58%)	4 (57%)
Mean survival time (range)	27 h (6–72 h)	Not applicable
Mean post-mortem delay (range)	56 h (3–120 h)	56 h (12–120 h)
Cause of Injury	Assault Fall Motor vehicle collision	Not applicable
Cause of death		
TBI	12 (100%)	0 (0%)
Acute cardiovascular death		3 (43%)
Inhalation gastric contents		1 (14%)
Acute death associated with amphetamine		1 (14%)
Bronchopneumonia secondary to malignancy		1 (14%)
Septicemia		1 (14%)